Combined real-time ultrasound plane wave compounding and linear array optoacoustics

Marc Fournelle*, Wolfgang Bost, Steffen Tretbar
Fraunhofer Institut für Biomedizinische Technik, Ensheimer Str. 48, D-66386 Sankt Ingbert

ABSTRACT

In optoacoustic imaging, the high optical contrast between different tissue types is combined with the high resolution and low scattering of ultrasound. Using adapted reconstruction algorithms, images of the distribution of light absorption in tissue can be obtained. Such as in any emerging modality, there is limited experience regarding the interpretation of optoacoustic images. For this reason, we developed a flexible hardware platform combining ultrasound imaging with optoacoustics. The system is based on the software processing of channel data and different types of reconstruction algorithms are implemented. It combines optoacoustic imaging based on linear arrays for detection with plane wave compounding ultrasound. Our system further includes a custom made probe based on a 7,5 MHz array, custom made fibre bundles for targeted light delivery and an acoustic coupling pad. The system was characterized on phantoms and first in-vivo datasets from subcutaneous vasculature were acquired.

Keywords: optoacoustics, vascular imaging, linear array, combined imaging, beamforming, coupling pad

1. INTRODUCTION

In optoacoustic imaging, the high optical contrast between different tissue types is combined with the high resolution and low scattering of ultrasound imaging. Signal generation results of subsequent conversion of light into heat and pressure due to light absorption processes in tissue [1, 2, 3]. Using adapted reconstruction algorithms, images of the distribution of light absorption in tissue can be obtained. This technique can be particularly valuable for imaging of subcutaneous blood vessels since haemoglobin is one of the best absorbing chromophores in biological tissue. Further, the intrinsic scalability of optoacoustic imaging allows the usage of this technique for imaging of microvasculature having diameters beyond the resolution limit of standard vascular imaging techniques such as Doppler ultrasound [4, 5, 6]. However, such as in any emerging modality, there is limited experience regarding the interpretation of optoacoustic images. For ease of understanding of optoacoustic images, the combination with an established modality such as ultrasound imaging is advantageous [7]. For imaging tasks, optoacoustic signals must be acquired at different positions on the sample surface which can either be realized by single element detection in combination with mechanical displacement [8,9] or multielement detection (array technology) [10,11]. Due to the complexity of achieving reliable acoustic coupling when the probe is mechanically moved – especially in the case of focused transducers – and due to considerations related to acquisition time and laser energy deposition, we developed an optoacoustic imaging system based on a linear ultrasound array for signal acquisition. The array is driven by a flexible hardware platform that allows to combine ultrasound imaging with optoacoustic techniques. The system is based on the software processing of channel data and different types of reconstruction algorithms are implemented. The system was characterized on phantoms and first in-vivo datasets from subcutaneous vasculature were acquired.

2. MATERIALS AND METHODS

2.1 Hardware Setup

The hardware platform is based on the latest generation of DiPhAS (Digital Phased Array System, Fraunhofer IBMT) combined with a Q-switched Nd:YAG laser system (Handy, Quanta System, Italy) operating at its fundamental wavelength of 1064 nm. The device can furthermore be combined with different laser sources such as OPOs by

* marc.fournelle@ibmt.fraunhofer.de; phone +49-6894 980 220; fax +49 6894 980 234; www.ibmt.fraunhofer.de

providing arbitrarily programmable trigger signals for laser flashlamp and Q-switch. For signal acquisition, a 7,5 MHz linear array transducer (Vermon SA, France) with a pitch of 300 µm has been used. The hardware platform DiPhAS has 128 independent transmit and receive channels and allows to digitize signals with 40 MSamples/s. The hardware concept relies on acquisition of channel data and fast data transfer to an integrated PC via Gigabit Ethernet for subsequent software-processing of data in a GPU (graphics processing unit). In the current setup, ultrasound or optoacoustic frames (having 128 lines) can be transferred and visualized with up to several hundred Hz depending on the image depth. However, the optoacoustic frame rate is limited to 20 Hz by the repetition rate of the currently used laser. The software of the device allows the selection of different presets in ultrasound and optoacoustic mode. For instance, the number of angles to be used in plane wave compounding can be selected. Further adjustable image parameters are the depth, the frequency of the transmit pulse in US mode, the depth-dependent amplification of received signals (TGC) or the number of pixels to be reconstructed during software beamforming. The hardware allows switching between optoacoustic and ultrasound mode in less than a second by choosing the corresponding preset. All relevant parameters (e.g. configuration of trigger signals, absence of transmit pulses, adaptation of beamforming algorithm) are stored in this preset. For targeted light delivery, the laser pulse is coupled into a custom made two-arm fibre bundle (Fiberoptic, Spreitenbach - CH). The bundle design has been chosen as a result of light distribution simulations based on a Monte Carlo model. Since the fibre output is placed adjacent to the transducer array, an illumination of structures placed directly in front of the aperture is not possible. Accordingly, no optoacoustic signals can be acquired from structures right in front of the aperture. For this reason, a custom made coupling pad with a thickness of 15 mm is connected to the transducer surface. The pad is made of a thermoplastic elastomer certified for clinical use which guarantees its safety when used in skin contact. Furthermore, it is optically transparent and has a low acoustic damping coefficient of approximately 0,2 dB/(MHz·cm), a sound velocity of 1471 m/s and a density of 0,78 g/cm³. For the sake of ergonomy, the transducer, the coupling pad and the fibre outputs are integrated in a custom made holder. A photograph of the probe with the fibre guides and the coupling pad attached is shown in figure 1. With all components assembled, the size of the probe approximately corresponds to that of a standard matrix array. The probe design foresees a slit for attachment of the tracking sensor of an electromagnetic tracking device that can be integrated for acquisition of 3D data. In preliminary experiments for freehand 3D optoacoustic imaging, the trackSTAR 2 system (Ascension, Milton - USA) was connected to the platform. The system has furthermore been mounted on a medical ultrasound cart (ITD GmbH, Unterhaching - Germany).

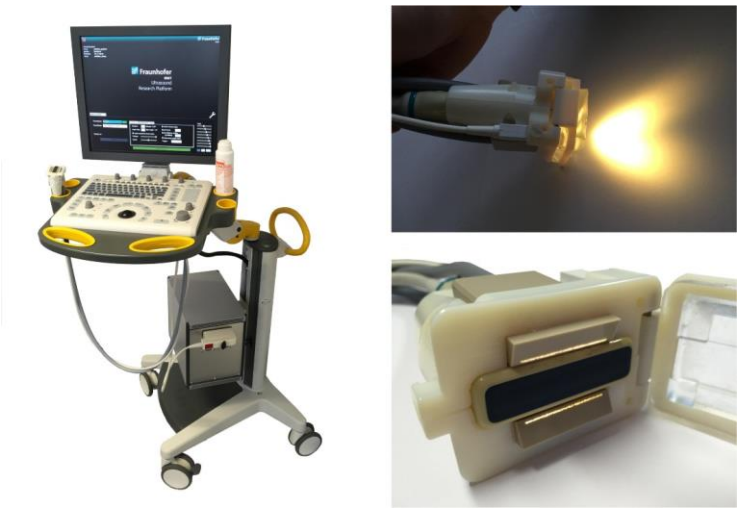

Figure 1. System overview and detail of transducer holder including custom made fibre bundle

2.2 Algorithms

In both imaging modes, channel data are acquired and transferred to a PC where a beamforming algorithm is implemented in a GPU. Massive parallelization in GPUs allows to perform channel data reconstruction in real time with frame rates higher up to hundreds of Hz. However, the actual frame rate of the system is limited to 80 Hz in ultrasound mode when a depth of 50 mm is chosen and to 20 Hz in optoacoustic mode due to the PRF of the laser. For the optoacoustic data, beamforming is performed with a conventional delay-and-sum algorithm with optional coherence, apodization and statistical filtering. In ultrasound mode, images are generated by plane wave compounding in order to take full profit of the channel data capabilities of the system. Different presets with optimal number of angles and angle

increment have been defined according to the results of preliminary simulations. Reconstruction of the individual data sets (one for each angle) is then as well performed based on conventional delay-and-sum beamforming and the compound image is generated by summation of the individual reconstructed data sets. When using the aforementioned acoustic coupling pad, a time-of-flight compensation is furthermore included in the beamforming algorithm in order to take into account the speed of sound of 1471 m/s in the elastomer. The effect of this correction is shown in figure 2a-b. Herein, a comparison of acoustic channel data acquired from a commercial ultrasound phantom (Model 040GSE, CIRS) reconstructed without (2a) and with (2b) sound speed compensation is shown. The effect on the PSF can clearly be recognized, especially in the structures being closest to the array. For generation of 3D images, the system first needs to undergo calibration. The used tracking system provides a 4x4 matrix defining the orientation and position of the tracker (integrated into the probe housing) in a global cartesian coordinate system. However, in order to be able to correctly register individual data frames (from US or OA) in this global system, the orientation and position of the frames is required. Therefore, a calibration step has been undertaken allowing to identify the correction matrix which performs the transformation from the tracker system into the image frame system. This matrix M (see fig. 2) is defined by the position of the array centre and the unit vectors x'', y'' and z'' as seen in the coordinate system of the tracker T (coordinate system Σ').

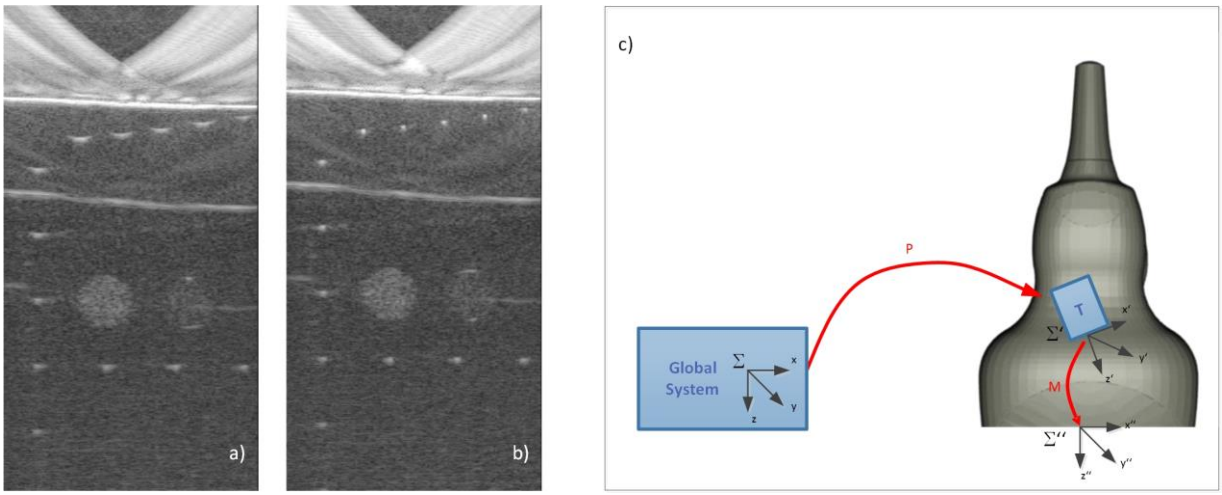

Figure 2. Influence of time of flight compensation on the quality of reconstructed image shown on acoustic data from a commercial ultrasound phantom (figure a and b). Transformation of coordinate systems for reconstruction of 3D volume data acquired with electromagnetic tracking (figure c)

These values are obtained by using a calibrated pointer needle allowing to acquire arbitrary positions on the array surface in the coordinate system Σ'. After acquiring a multitude of positions of the array surface, a best plane fit is performed and the surface normal is defined as z''. The corners of the array surface furthermore allow to obtain the position of the array centre as well as x''. Finally, y'' is obtained as a cross product of z'' and x''.

3. RESULTS

For assessment of the system´s performance, wire phantoms were imaged in both modalities. For this purpose, an optically absorbing wire was moved in axial direction and channel data were acquired in each step. The wire phantom was immersed in a 6% milk in water mixture in order to mimic optical scattering properties of biological tissues. At each step (corresponding to different depths), the optoacoustic channel data were reconstructed with conventional beamforming with optional filtering. The signal to noise ratio and the full-width-half-maximum (FWHM) of the point-spread-function (PSF) were assessed for each depth and the influence of additional filter algorithms was evaluated.

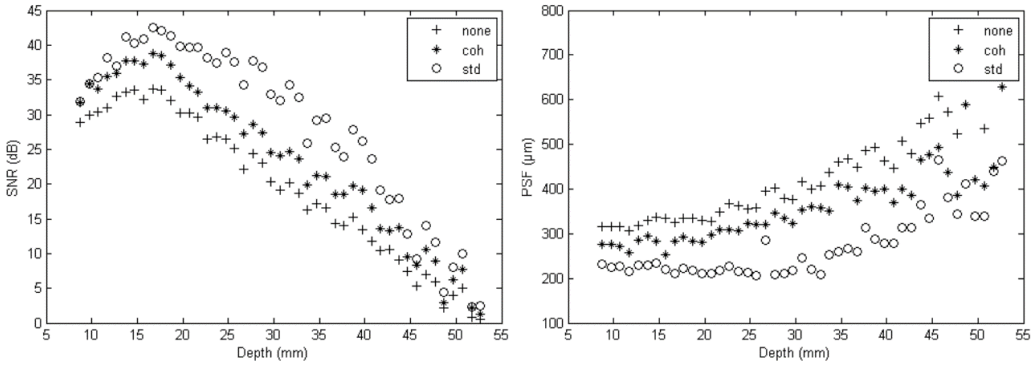

Figure 3. Depth dependent FWHM of the PSF and SNR using a 7,5 MHz PZT array in the optoacoustic mode

The results depicted in figure 3 show that absorbing structures can be detected with adequate SNR up to depths of approximately 45 mm in highly scattering media. Furthermore, the results show the impact of additional filter algorithms during sum-and-delay beamforming. While the FWHM of the PSF is in the range of 330 µm for the first 25 mm in depth in the case of conventionally beamformed optoacoustic images, coherence and statistical filtering allow to decrease the FWHM down to ~ 290 µm and ~210 µm respectively. In a next step, in order to have a more realistic model for assessment of the penetration depth in biological media, a vessel like phantom was embedded in chicken breast tissue. The vessel phantom consists of PVCP (Polyvinylchloride plastisol) whose optical absorption coefficient was enhanced with black dye.

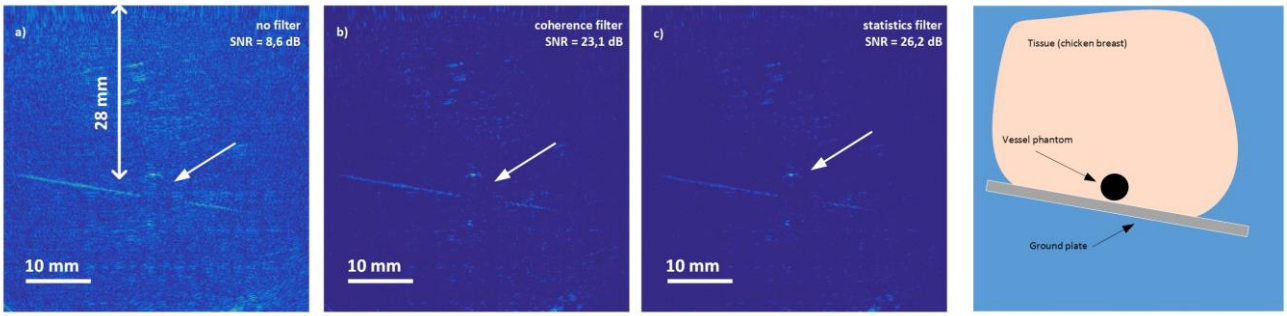

Figure 4: Vessel mimicking PVCP phantom embedded in chicken breast tissue reconstructed using different filter algorithms in optoacoustic mode

All optoacoustic phantom experiments haven been performed without having to fall back on averaging with a laser fluence of approximately 15 mJ/cm² at the used wavelength of 1064 nm. The optoacoustic image clearly allows to recognize the ground plate on which the vessel model and the chicken breast tissue are positioned. The upper boundary of the vessel phantom can as well clearly be delineated in a depth of 28 mm. The SNR was assessed as the ratio between the maximum of the phantom signal divided by the maximum of the background signal (expressed in dB). Depending on the used reconstruction algorithms, a SNR between 8,6 dB and 26,2 dB has been obtained. In a further set of phantom experiments, the ability of the DiPhAS system combined with the tracking tool trackSTAR for 3D freehand imaging was assessed. A phantom consisting of different black absorbing wires immersed in a 6% milk in water mixture in different depths was used for this purpose.

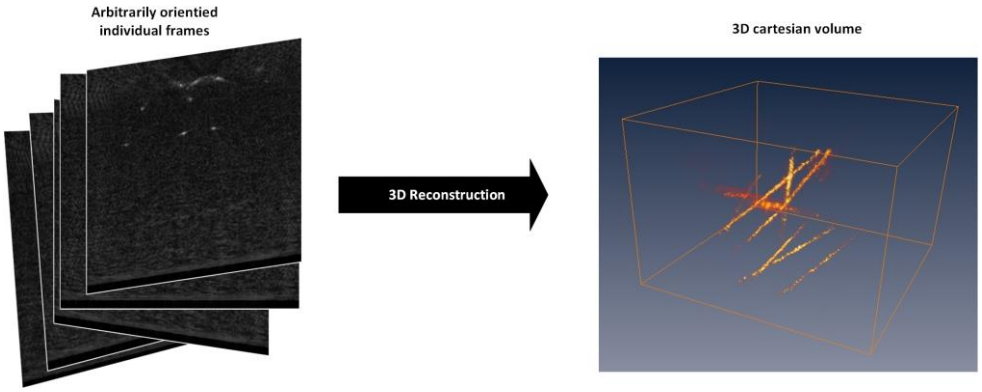

Figure 5: 3D reconstruction of wire phantom based on freehand acquisition of individual 2D optoacoustic data frames

For generation of the 3D volume shown in figure 5, a total of 512 2D optoacoustic data sets has been acquired. For generation of the cartesian 3D volume, a C# software tool has been implemented which loads individual 2D frames, computes the location of individual pixels in the global coordinate system (x_p, y_p, z_p) based on the location of the pixel within the frame (x_p'', 0, z_p'') and the transformation matrix of the latter, and adds the pixel value to the corresponding voxel. According to this procedure, a volume consisting of 223 x 222 x 328 voxels of each 300 µm edge length has been generated and visualized using AMIRA (Visage Imaging, Richmond - Australia). For improvement of lateral resolution, the 2D data has been beamformed under consideration of the above mentioned statistics filter.

3.1 In-vivo experiments

In a next step, combined imaging of subcutaneous vasculature was performed in the hand of a proband. In all optoacoustic measurements, optical fluency below 20 mJ/cm² far below the ANSI safety threshold of 100 mJ/cm² at 1064 nm was used. The measurements were performed with the above mentioned acoustic coupling pad and were repeated with the hand immersed in a water tank in order to assess the influence of the pad. The comparison shows that the contour of the finger can – obviously – not be reconstructed accurately when using the pad since acoustic coupling is limited to the top side of the finger. Furthermore, the upper part of the acoustic images (first 15 mm) is affected with artefacts which are characteristic for plane wave compounding when an offset is present between the transducer surface and the investigated object. Ultrasound images presented in figure 6 were all generated with plane wave compounding using 7 angles.

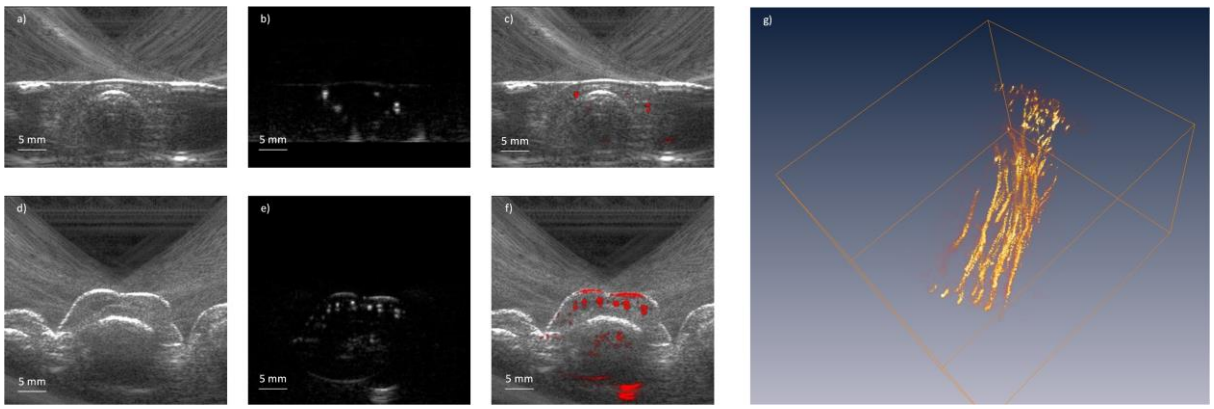

Figure 6. Combined acoustic and optoacoustic imaging of vasculature in a proband´s finger using the acoustic coupling pad (upper row) and using water coupling (lower row). Freehand 3D optoacoustic volume data from blood vessels in the forearm of a human proband (figure g) acquired with 7,5 MHz array and 1064 nm laser pulse.

Since the acoustic velocity in the pad is comparable to that in water, there is no image deterioration induced by the usage of the pad and vessels can accurately be reconstructed (see figure 6b). A direct assessment of the effect of the pad on the SNR cannot be performed since distinct vessels with unknown radius have been imaged. However, the analysis of signal

amplitudes shows that the influence of the pad is limited since SNRs of 58 and 63 dB have been measured respectively with and without coupling pad. Finally, the system has been used for freehand 3D imaging of the vasculature in the forearm of a proband. In this experiment, the hand-held probe is directly coupled to the skin of the proband using commercially available ultrasound coupling gel. Laser and ultrasound parameters remained unchained in comparison to the already described experiments. Individual 2D frames were acquired without averaging and reconstructed with a resolution of 512 x 1024 pixels (in lateral and axial dimension respectively) while using the statistics filter during beamforming. A total of 2415 frames have been acquired, which corresponds to an acquisition time of approximately 120 s given the limitation of the optoacoustic resulting of the laser PRF of 20 Hz. These frames have been reconstructed to a volume of 563 x 523 x 349 voxels with an edge length of 300 µm which then has been visualized using AMIRA. A 3D representation of the vessel network in the forearm is given in figure 7g.

4. CONCLUSION

A system for combined imaging based on plane wave compounding and optoacoustic imaging using linear array transducers has been developed and characterized using wire phantoms and first in-vivo measurements on probands. The system includes a custom made integrated probe based on a linear array transducer, fibre guides for targeted light delivery and a coupling pad. The results show the limitations and benefits of the approach involving an acoustic coupling pad. Especially when irregular contours need to be imaged, an approach involving a water tank is preferred since acoustic coupling can only partially be guaranteed in such cases using a pad. The results further show that a loss in SNR in the range of 2 to 5 dB can be expected as a result of using an acoustic coupling pad. However, in applications where a high SNR is given and structures placed directly under the skin need to be visualized (e.g. subcutaneous vasculature), a setup with an integrated coupling pad such as proposed allows convenient freehand scanning without the need for water immersion. The system´s suitability for freehand 3D imaging has furthermore been demonstrated on phantoms and in-vivo data from a human proband.

5. ACKNOWLEDGMENT

The authors want to acknowledge the “Staatskanzlei des Saarlandes” for funding in the context of the “Landesforschungsförderungsprogramm”.

REFERENCES

[1] Xu M., Wang L.V.,”Photoacoustic imaging in biomedicine,” Rev Sc Inst 77, 041101 (2006)
[2] Kim C., Favazza C., Wang L.V., “In vivo photoacoustic tomography of chemicals: high resolution functional and molecular optical imaging at new depths,” Chem. Rev. 110(5), 2756-2782 (2010)
[3] Wang L., Song H.,“Photoacoustic tomography: in vivo imaging from organelles to organs,” Science 335(6075), 1458-1462 (2010)
[4] Zhang E.Z., Laufer J.G., Pedley R.B., Beard P.C. ,”In vivo high-resolution 3D photoacoustic imaging of superficial vascular anatomy,” Phys. Med. Biol.54, 1035–1046 (2009)
[5] Hai P., Yao J., Maslov K.I., Zhou Y., Wang L.V., “Near infrared optical resolution photoacoustic microscopy,” Opt. Lett. 39(17), 5192-5195 (2014)
[6] Yang Z., Chen J., Yao J., Lin R., Meng J., Liu C., Yang J., Li X., Wang L., Song L. “Multi-parametric quantitative microvascular imaging with optical resolution photoacoustic microscopy in vivo,” Optics Express. 22(2), 1500-1511 (2014)
[7] Kim C., Erpelding T.N., Jankovic L., Pashley M.D., Wang L.V., “Deeply penetrating in vivo photoacoustic imaging using a clinical ultrasound array system,” Biomed. Optics Express. 1(1), 130227 (2010)
[8] Bost W., Lemor R., Fournelle M., “Optoacoustic Imaging of subcutaneous microvasculature with a class one laser,” IEEE Trans. Med. Im. 33(9), 1900-1904 (2014)
[9] Wang L., Maslov K., Yao J., Rao B., Wang L., “Fast voice-coil scanning optical resolution photoacoustic microscopy,” Opt. Lett. 36(2), 139-141 (2011)
[10] Schwarz M., Buehler A., Ntziachristos V., “Isotropic high resolution optoacoustic imaging with linear detector arrays in bi-directional scanning,” J. Biophotonics 8(1), 60-70 (2015)
[11] Held G., Preisser S., Akarcay H.G., Peeters S., Frenz M., Jaeger M., “Effect of irradiation distance on image contrast in epi-optoacoustic imaging of human volunteers,” Biomed. Optics. Express 5(11), 3765-3780 (2014)